THE ASTROPHYSICAL JOURNAL, 492:323–341, 1998 January 1

DISK ACCRETION RATES FOR T TAURI STARS[1]

ERIK GULLBRING, LEE HARTMANN, CESAR BRICEÑO,[2,3] AND NURIA CALVET[3]
Harvard-Smithsonian Center for Astrophysics, 60 Garden Street, Cambridge, MA 02138;
egullbring@cfa.harvard.edu, lhartmann@cfa.harvard.edu
Received 2997 May 27; accepted 1997 August 12

ABSTRACT

We present new measurements of disk accretion rates for T Tauri stars in the Taurus molecular cloud complex. Our results are based on intermediate-resolution spectrophotometry from 3200 to 5200 Å, which is used to derive the excess hot continuum emission produced by accretion onto the central star. Previous estimates of T Tauri accretion rates in the literature differ by as much as 1 order of magnitude; our measurements agree better with the lowest estimates, and we discuss the problems and systematic effects that led to the previous disagreement. In particular, we note that the stellar photospheric emission from nonaccreting T Tauri stars exhibits color anomalies compared to main-sequence stars; these anomalies make the estimated extinction depend upon the color index used. We argue that the $V-R$ index is a reasonable compromise to match with optically derived spectral types, and that $V-I$ and $V-J$ are much more likely to be biased by cooler companion stars and starspots. We develop a calibration with which approximate mass accretion rates can be derived for T Tauri stars based on broadband photometry and spectral types, which should enable accretion rates to be estimated for large samples with greater ease.

Subject heading: accretion, accretion disks — stars: pre–main-sequence

1. INTRODUCTION

The strong excess emission of some low-mass, pre–main-sequence T Tauri stars is thought to be produced by accreting circumstellar disks (Lynden-Bell & Pringle 1974; see the reviews by Appenzeller & Mundt 1989 and Bertout 1989). The excess luminosity depends upon the mass accretion rate, which is an important parameter for understanding the evolution of both stars and disks. Unfortunately, excess luminosities in T Tauri stars are difficult to estimate; current uncertainties and potential systematic errors have limited progress in understanding disk evolution.

Although disks should be self-luminous owing to the release of accretion energy, it proves to be difficult to measure accretion rates from infrared disk emission in most T Tauri stars because irradiation from the central star is often a larger heat source for the disk than viscous dissipation (see, e.g., Kenyon & Hartmann 1987). For this reason most estimates of accretion rates in T Tauri stars are derived from the hot continuum radiation produced as disk material lands on the stellar surface (Bertout, Basri, & Bouvier 1988; Basri & Bertout 1989; Hartigan et al. 1990, 1991; Valenti, Basri, & Johns 1993, hereafter VBJ; Hartigan, Edwards, & Ghandour 1995, hereafter HEG). Measurements of the hot continuum excess require distinguishing between accretion-produced emission and stellar photospheric emission, which is difficult when the accretion luminosity is small in comparison with the stellar luminosity. The difficulty in making excess luminosity measurements is greatly increased by the need to make significant extinction corrections, which require a knowledge of the colors of both the underlying star and the hot excess continuum. These problems, plus differing assumptions concerning the geometry of accretion, have resulted in greatly differing estimates of accretion rates in the literature. Two of the most recent, careful, and systematic studies, those of VBJ and HEG, differ in accretion rates for the same stars by as much as 1 order of magnitude.

Because of the large uncertainties in mass accretion rates for T Tauri stars and the importance of understanding mass fluxes for disk evolution, we decided to pursue an observational approach to the problem that attempts to combine the strengths of VBJ and HEG. Like VBJ, we obtained flux-calibrated spectra that cover the blue spectral region from 3200 to 5200 Å, which provide simultaneous spectral coverage of wavelength regions where much of the accretion luminosity is thought to be radiated. Our spectra have slightly higher resolution than those of VBJ, which makes it easier to determine the depths of stellar photospheric features; from the amount by which stellar absorption features are "veiled," we are able to make estimates of the relative emission of star and hot continuum as a function of wavelength (as HEG did from much higher resolution spectra).

The resulting mass accretion rates for 14 accreting T Tauri stars in the Taurus cloud complex generally agree better with VBJ than with HEG, although with considerable scatter. We show that the systematic discrepancies between VBJ and our findings on the one hand and HEG on the other arise from two primary sources: differing extinction estimates, which are related to color differences between T Tauri photospheres and normal dwarf stars, and differences in the assumed accretion geometries. While differences in geometrical assumptions and reddening enhance the differences in the accretion rates for HEG, these factors tend to cancel for VBJ.

We show that the excess radiation in the U-magnitude band is closely related to the accretion luminosities derived here. Using this result, we demonstrate that broadband photometry and spectral types may be combined to produce accretion rate estimates for other stars without requiring detailed spectrophotometry. The magnitudes of

[1] Research reported herein was performed with the Multiple Mirror Telescope, which is jointly operated by the Smithsonian Institution and the University of Arizona.

[2] Also at Postgrado de Física, Universidad Central de Venezuela, Caracas, Venezuela.

[3] Also at Centro de Investigaciones de Astronomía (CIDA), Mérida, Venezuela.

TABLE 1

EMISSION-LINE EQUIVALENT WIDTHS AND BALMER JUMPS

Object	Spectral Type	Class	Hβ[a]	Hγ[a]	Hδ[a]	Hε + Ca II H[a]	Ca II K[a]	Balmer Jump[b]
BP Tau	K7	CTTS	28.2	21.2	17.7	22.2	14.0	1.3
AA Tau.....	K7	CTTS	6.7	13.5	14.7	21.6	11.2	1.0
CW Tau	K3	CTTS	43.9	23.3	8.3	38.0	70.3	1.6
CY Tau.....	M1	CTTS	50.2	39.3	37.2	51.2	25.4	1.8
DE Tau.....	M2	CTTS	32.6	25.5	20.3	57.9	69.2	1.9
DF Tau.....	M1	CTTS	33.4	24.0	25.2	28.4	14.9	1.9
DG Tau	K7–M0	CTTS	20.3	9.9	4.1	19.6	20.4	1.2
DK Tau	K7	CTTS	20.5	14.4	9.9	24.2	19.7	1.0
DL Tau.....	K7	CTTS	58.4	33.5	28.0	75.4	85.9	2.3
DN Tau	M0	CTTS	9.1	13.2	14.3	20.8	13.1	0.8
DO Tau	M0	CTTS	35.1	13.1	13.2	76.7	63.2	2.4
DQ Tau	M0	CTTS	17.4	20.9	14.8	19.9	17.3	0.6
DR Tau	K7	CTTS	11.2	5.5	3.3	9.7	15.9	1.4
DS Tau.....	K5	CTTS	22.6	15.6	11.9	16.7	11.4	1.1
FM Tau	M0	CTTS	31.6	20.3	16.8	19.2	9.9	1.2
FP Tau	M4	WTTS-CTTS	5.4	8.2	8.5	18.9	16.6	0.6
GG Tau	K7	CTTS	24.5	22.3	19.8	42.5	46.5	1.6
GI Tau	K6	CTTS	15.2	16.1	13.9	22.8	8.8	1.0
GK Tau	K7	CTTS	8.1	13.7	11.6	22.8	19.9	0.8
GM Aur.....	K7	CTTS	26.3	20.4	18.4	18.5	12.3	1.1
HBC 351	K5	WTTS	0.6	<0	<0	−2.1	<1	0.4
HN Tau	K5	CTTS	39.7	22.4	6.6	49.1	65.3	1.4
IP Tau.....	M0	CTTS	6.3	12.2	11.7	16.5	9.5	0.8
LkCa 7	K7	WTTS	<2	<1	<1	7.6	8.9	0.4
RW Aur	K3	CTTS	8.4	3.4	2.3	7.8	22.1	0.7
UY Aur.....	K7	CTTS	21.1	17.2	16.7	22.4	13.9	1.2
V819 Tau.....	K7	WTTS	<1.5	<1	<1	4.5	6.5	0.1
V836 Tau.....	K7	WTTS	2.1	3.0	<1	6.8	7.9	0.1

[a] Equivalent widths are given as negative values in Å.
[b] The Balmer jump is measured as the flux ratio between 3600 Å and 4000 Å.

mass accretion in T Tauri stars have important implications for understanding the evolution of protoplanetary disks, as will be developed in a subsequent paper (Hartmann et al. 1998).

2. OBSERVATIONS AND DATA REDUCTION

Medium-resolution spectrophotometry of pre–main-sequence stars in the Taurus-Auriga cloud were obtained with the Multiple Mirror Telescope (MMT) in 1996 December. The sample contained three weak-line T Tauri stars (WTTSs) and 26 classical (strong emission) T Tauri stars (CTTSs) that span a large range of excess emission (HEG) and spectral types (Kenyon & Hartmann 1995; hereafter KH). The stars in the sample are presented in Table 1. In addition, spectra of a number of spectrophotometric and main-sequence standard stars were taken. The observations were made using the blue channel of the MMT spectrograph with the 800 line grating. The spectral dispersion was 0.75 Å pixel^{-1}, and the wavelength coverage spanned 3200 to 5400 Å. We used a 5″ slit to obtain spectrophotometry with ∼1″ seeing. With such a large slit, the spectral resolution was somewhat seeing- and guiding-dependent; we estimate typical resolutions to be ∼3 Å. Integration times ranged from 2 to 12 minutes for the target objects.

The data were reduced using standard IRAF routines.[4] HeNeAr lamp spectra were used to calibrate the wavelength scale with a relative accuracy of less than 1 pixel. The observations were collected during excellent photometric conditions, which permitted good flux calibration. Spectrophotometric standard stars were selected from the intensified image dissector scanner (IIDS) standards listed in IRAF (Massey, Valdes, & Barnes 1992).

The flux errors can arise from wavelength-dependent errors, variable transparency, and slit losses, which may or may not be wavelength dependent. The slit was rotated to minimize wavelength-dependent slit losses due to atmospheric dispersion, but gray- or wavelength-independent slit losses are likely. Therefore, when determining the system sensitivity as a function of wavelength from the spectrophotometric standards, two kinds of errors occur: (1) wavelength independent-observation-to-observation residuals that can be accounted for by grayshifting the data, that is, shifting the mean sensitivity of each observation in order to match the observation of highest sensitivity; and (2) scatter of data points after the grayshift. The sensitivity function was derived by fitting a spline function (of order 6) to the flux responses of the standard stars. The measurements showed that the observation-to-observation residuals were small in the spectral region $3500 < \lambda < 5300$ Å, showing shifts with respect to the mean fluxes of $\leq 7\%$. The intrinsic scatter of the flux measurements at each wavelength, after grayshifting the data, was ∼5% (and only slightly larger even when not employing systematic grayshifts).

At the very blue ($\lambda < 3400$ Å) and red ($\lambda > 5300$ Å) ends of the spectra, the accuracy of the flux calibration was lower. After the grayshift, the standard flux measurements at the blue end showed a scatter of $\leq 12\%$ together with a small systematic shift of $\leq 15\%$. At these short wavelengths a less accurate flux calibration is expected, since the atmospheric transmission decreases the count rates and since it is also more sensitive to the adopted atmospheric extinction law. We measured the extinction law by observing flux stan-

[4] IRAF is distributed by the National Optical Astronomy Observatories, which is operated by the Association of Universities for Research in Astronomy, Inc., under contract to the National Science Foundation.

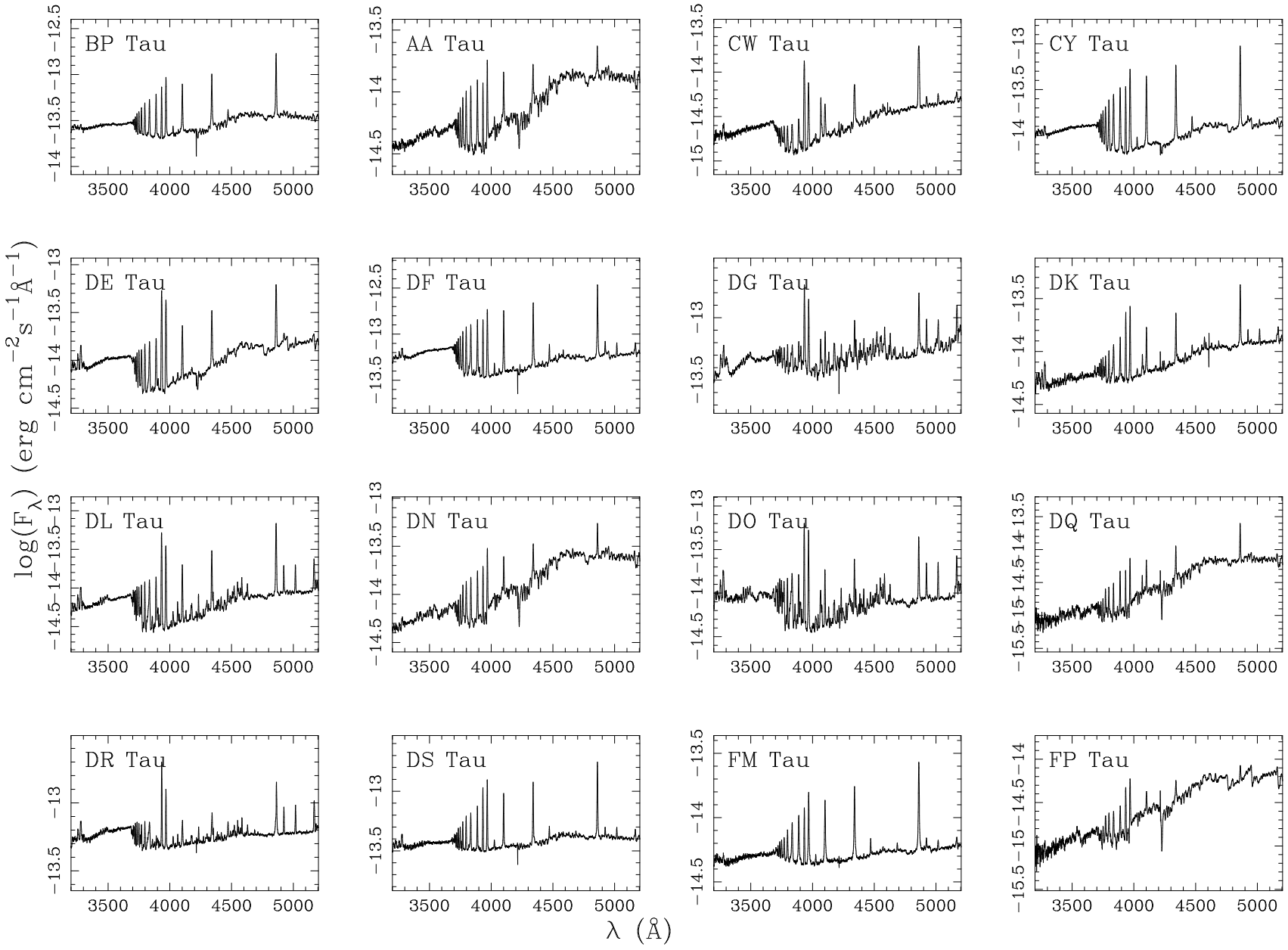

FIG. 1.—Observed T Tauri stellar spectra

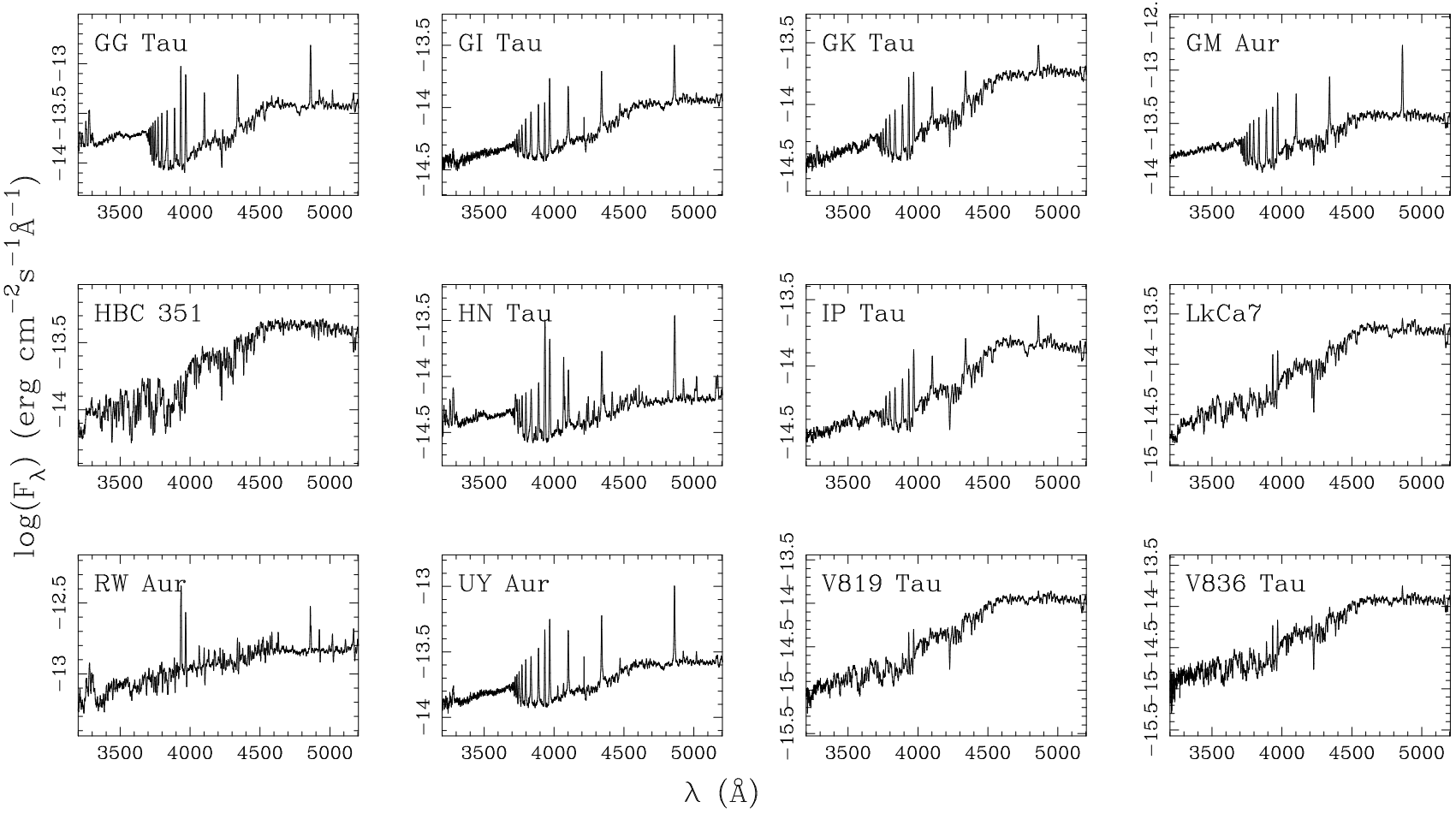

FIG. 1.—*Continued*

dards over a large range of air masses. The difference between the flux calibration obtained by applying our derived extinction and the standard KPNO extinction law, given in IRAF, was less than 1% in the red and ~4% in the blue part of the spectrum. At the red end ($\lambda > 5300$ Å), vignetting in the spectrograph affected the flux calibration, in particular the fit of the sensitivity function. In the following, we will therefore consider only the part of the spectra at wavelengths shorter than 5300 Å.

Figure 1 presents the flux-calibrated spectra of the stars in our sample, many with strong hydrogen emission in the continuum and lines. In Table 1 we present the observed equivalent widths of the H and Ca II lines and Balmer jumps of the observed spectra. The Balmer jumps are measured as the ratio between the fluxes at 3600 and 4000 Å (regions relatively free of emission lines).

3. ANALYSIS

3.1. *Overview*

The low-mass, pre–main-sequence stars can be divided into the weak-emission WTTSs and the strong-emission CTTSs. The WTTSs, which do not show the near-infrared excess emission that can be attributed to a close circumstellar disk, also show no discernible hot continuum emission at optical wavelengths, whereas the CTTSs show near-infrared excess emission as well as hot continuum emission (Hartigan et al. 1990). This correlation between near-infrared excess and optical-ultraviolet hot continuum emission is the basis for identifying accretion from the circumstellar disk as the energy source for the hot continuum.

Originally, the hot continuum excess was attributed to emission from the boundary layer at the interface between the Keplerian disk and the slowly rotating T Tauri star (Lynden-Bell & Pringle 1974). This picture has now been replaced by a model of magnetospheric accretion in which the stellar magnetic field disrupts the disk at several stellar radii; accreting material is channeled along field lines, falling in freely until it shocks at the stellar surface, where the hot continuum emission is produced (Königl 1991; Camenzind 1990). The observational basis for this picture is discussed in Hartmann (1994). The stellar magnetosphere model is attractive because it simultaneously explains (1) hot spots rotating with the star (because of its magnetic field structure); (2) the absence of inner disk emission in some stars (Bertout et al. 1988); (3) the slower rotation of stars with inner disks (Bouvier et al. 1993; Edwards et al. 1993), which can be explained by the disk torques communicated to the star by the magnetic field (Königl 1991; Shu et al. 1994); and (4) the emission profiles of permitted lines, in particular inverse P Cygni redshifted absorption features (Edwards et al. 1994), which can be accounted for by emitting gas in free fall along the magnetosphere (Hartmann, Hewett, & Calvet 1994).

We assume that the stellar magnetic field channels the accretion flow onto a finite (and small) spatial area of the stellar surface, so that most of the stellar photosphere is unaffected by the accretion process. The spectrum of a CTTS then consists of the sum of the stellar photospheric emission plus a hot emission component whose spectrum is unknown a priori. Both components are reddened by interstellar extinction. To derive accretion luminosities it is necessary to disentangle the two emission components while solving for the extinction and then make a correction for the excess emission at unobserved wavelengths.

3.2. *Methodology*

The presence of excess emission causes the depth of the stellar photospheric absorption lines to decrease, compared to a standard (nonaccreting) stellar spectrum. To the extent that the veiling is due to continuous emission, measurements of lines at different wavelengths yield the ratio of hot excess emission to stellar photospheric emission as a function of wavelength; this information can be used to estimate the spectral shape of the excess relative to the star and the extinction to the system if the intrinsic colors of the template stellar photosphere are known (see Hartigan et al. 1989).

For our program objects, we estimated the relative veiling, r, defined as the ratio between the excess, F^E, and stellar fluxes, F_c^*, in the continuum (Hartigan et al. 1990), by measuring the line-to-continuum values for a number of absorption features in both the veiled and the template spectra. The relation between r and the line-to-continuum measurements (assuming F^E is constant over a wavelength region covering a line and its adjacent continuum) is

$$r = \frac{F_l^o/F_c^o - F_l^*/F_c^*}{1 - F_l^o/F_c^o}, \tag{1}$$

where l and c refer to the line and the continuum of the veiled object (o) or of the stellar photosphere ($*$). It is important to note that r is a reddening-independent parameter (under the assumption that the reddening is the same for the line as for the adjacent continuum), and it is also insensitive to systematic errors in the flux response function.

The largest uncertainties in the measurement of r are not due to the photon and/or readout noise but instead to the low spectral resolution, which makes it difficult to estimate the amount of filling in of nonphotospheric emission lines in the absorption features and to estimate spectral type mismatches. In particular, the presence of iron emission lines makes obtaining the veiling measurements in the region around 4500 Å very difficult for many stars. The most suitable photospheric lines for measuring r are in the region 4150 Å $< \lambda <$ 4440 Å and 4700 Å $< \lambda <$ 5200 Å. At the red end of the spectra, both vignetting and the presence of iron lines make it difficult to obtain reliable values for r. Also, as will be discussed in § 3.3, the depth of the strong TiO feature at 4700–4850 Å is affected by causes other than just veiling. Even for stars with very strong line emission, like HN Tau and GG Tau, enough absorption features could be found to get reasonable measurements of the veiling.

If the stellar flux, F_c^*, is known, the excess flux, F^E, is given by the definition of r as $F^E \equiv rF_c^*$. Assuming that the CTTS has the same photospheric emission as the template star (t), then at wavelength bin i,

$$F_i^* = C_1 F_i^t 10^{0.4A_i^t}, \tag{2}$$

where C_1 is a (wavelength-independent) constant that takes into account the different solid angles subtended by the object and template stars, and F_i^t and A_i^t are the observed flux and interstellar extinction of the template star. The observed CTTS flux is then

$$F_i^o = (F_i^* + F_i^E)10^{-0.4A_i^o} = C_1 F_i^t 10^{0.4(A_i^t - A_i^o)}(1 + r_i), \tag{3}$$

where A_i^o is the extinction toward the object. Assuming that A_i^t is known, then two unknowns remain: C_1 and A_i^o.

Equation (3) can be rewritten as

$$A_i^o = 2.5 \left\{ \log \left[\frac{F_i^t}{F_i^o} (1 + r_i) \right] + 0.4 A_i^t + \log C_1 \right\} . \quad (4)$$

Assuming that C_1 is known, one measurement of A_i^o is sufficient to determine A_V^o, if the extinction follows some known law. In practice, N lines are measured so that N values of A_V^o are found.

If C_1 is not known a priori, equation (4) provides N equations for the two unknowns, C_1 and A_V^o. Since N is normally greater than 2, equation (4) gives an overdetermined set of equations. Typically, the number of photospheric lines usable for veiling measurements ranges from 5 to 15. Writing equation (4) as

$$2.5 \log \left[\frac{F_i^t}{F_i^o} (1 + r_i) \right] = w_i (A_V^o - A_V^t) 2.5 \log C_1 , \quad (5)$$

where $w_i = A_i / A_V$, it is possible to make a least-squares fit to a straight line for the quantity $2.5 \log [F_i^t / F_i^o (1 + r_i)]$ versus w_i. The slope of the fitted line will give $A_V^o - A_V^t$ and therefore A_V^o if A_V^t is known, and the zero point will provide a value for C_1. As an example, we show in Figure 2 (*top*) the values for the relative veiling of BP Tau, together with (*bottom*) the fit of equation (5) . For objects with A_V^o similar to A_V^t, the slope will typically be smaller than the scatter in the values of $2.5 \log [F_i^t / F_i^o (1 + r_i)]$, which implies a badly determined value for C_1 or, rather, bad simultaneous solutions of C_1 and A_V^o. A way around this problem is to normalize equation (4) to a specific wavelength bin, j; this achieves a more robust relation by forcing the dependent and independent parameters to have the same zero point:

$$\log \left[\frac{F_j^t}{F_i^t} \frac{F_i^o}{F_j^o} \frac{(1 + r_j)}{(1 + r_i)} \right] = 0.4 (A_V^o - A_V^t)(w_i - w_j) . \quad (6)$$

Once A_V^o is determined by a least-squares fit of equation (6), then C_1 can be determined as an average for the N lines. In principle, one could solve equation (6) directly for two wavelengths, giving $N - 1$ solutions for A_V^o. One such solution would look like

$$A_V^o = \frac{2.5}{(w_i - w_j)} \log \left[\frac{F_i^t}{F_j^t} \frac{F_j^o}{F_i^o} \frac{(1 + r_i)}{(1 + r_j)} + A_V^t \right] . \quad (7)$$

It is seen that equation (7) has a singularity at $w_i = w_j$, which just reflects the problem that the extinction cannot be determined from two very close wavelengths or for a flat extinction law. It is possible to solve equation (7) directly for $i \neq j$, but it is difficult to determine when the presence of the singularity will affect the solution, i.e., the scatter of the data gives a high uncertainty in the solution for $w_i \sim w_j$.

The error for A_V^o is determined from the goodness of fit to the straight line. The error is dominated by nonstatistical errors related to "bad" photospheric lines and/or measurement errors. The error of C_1 is determined from either the scatter of the A_V^o values for each line or from the error induced by the line fit of equation (5), whichever method was used.

In practice, A_V^o and C_1 are determined using the following steps:

1. Make a preliminary fit for A_V^o for a given C_1 by equation (4), giving N systematically wrong values of A_V^o but with a low scatter. These values are used to identify "bad" photospheric lines that give values that deviate strongly from the mean.
2. For the "good" lines, A_V^o and C_1 are calculated with the method described in this section.
3. A last check is done by looking at the excess spectrum and assuming that it is linear between $\sim$4000 and 5000 Å. That is to say that there should be no contribution by the underlying star, which flux-drops at $\sim$4500 Å. Normally, only adjustments of the A_V^o and C_1 values within the errors (given from the scatter by the unweighted data points) are sufficient to achieve this.

Since the statistical errors in the spectral region of interest for measuring the veiling only give errors of the order of $\sim$10% in $\log [(1 + r_i) F_i^t / F_i^o]$, the uncertainties in the A_V, C_1 fits are almost solely determined by the deviations in the r-measurements caused by the unknown amounts of filling in of the absorption features by emission lines.

3.3. *The Colors of WTTSs and Extinction Estimates*

The above method assumes that the intrinsic spectrum of the accreting T Tauri star can be accurately represented by that of the template star. We assume that, by matching spectral types, we can use a standard, nonaccreting stellar spectrum for the photospheres of accreting T Tauri stars. In principle, the best standards are provided by WTTSs of the same spectral type and gravity. In practice we had to supplement our WTTSs with nearby main-sequence dwarfs to obtain an adequate range of spectral types (or effective temperatures).

One of the unexpected results of our analysis was the realization that the assumption of a standard stellar spec-

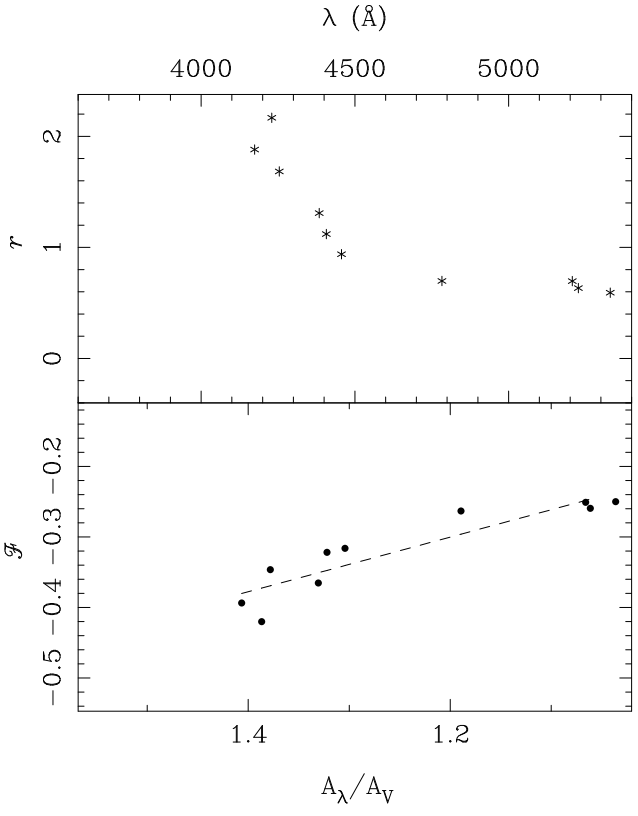

FIG. 2.—*Top*: Measured values for the relative veiling of BP Tau. *Bottom*: Fit of the values given by eq. (5) for BP Tau. The ordinate displays the quantity $2.5 \log [(1 + r) F^t / F^o]$ for each wavelength (see text for details).

trum involves not only an appropriate spectral type match but also a good estimate of the extinction of the template star. This is not an issue when using nearby Gliese (Gl) dwarfs as templates, but it is important when using WTTS templates, which may have substantial reddening.

In particular, the K7 WTTS LkCa 7 has frequently been used as a standard star because it is bright and because its spectral type is similar to those of many CTTSs in Taurus (Hartigan et al. 1990, 1991; HEG). In our initial reductions, we used LkCa 7 and its estimated extinction, $A_V \sim 0.6$, from KH. The excess spectrum derived from these assumptions showed very blue Paschen continuum slopes. While the resulting excess emission spectra were very similar to those derived by Hartigan et al. (1991) for some objects, the Paschen continuum slopes in others imply that the flux extrapolates to zero (or negative) values just beyond our wavelength coverage. This behavior suggests that the assumed template star colors are incorrect and prompted us to review the use of LkCa 7 as a template.

Figure 3 compares the colors of three WTTSs of similar spectral type—LkCa 7, V819 Tau, and V830 Tau—with colors of standard dwarfs and giants. It is evident that the $B-V$ versus $V-R$ colors of LkCa 7 are anomalous and cannot be explained by standard stars with any reddening. A similar effect is suggested in the $V-R$ versus $R-I$ color-color plot. Adopting the K7 spectral type and the standard colors given in KH and using the mean photometry listed in KH, the extinction of LkCa 7 estimated from its $B-V$ color is $A_V = -0.03$ mag, from $V-R$, $A_V \sim 0.45$ mag, and from $V-I$, $A_V \sim 0.9$ mag. The $V-I$ index is not a very good estimator of A_V, since the amount of dereddening becomes very sensitive to the spectral type classification. In part, the different visual extinctions (A_V) resulting from different color indices may be caused by the binary nature of LkCa 7 (Leinert et al. 1993); there may be other reasons, as discussed below.

Given these problems with the colors of LkCa 7, we used the other K7 WTTS template in our sample, V819 Tau. This star is also a binary, but the K-band brightness of the secondary is only 3.5% of that of the primary (Leinert et al. 1993). The values for the interstellar extinction of V819 Tau in the literature range from 1.1 to 1.35 mag (VBJ; Hartigan et al. 1991; HEG; KH). The average broadband colors of V819 Tau from Herbst, Herbst, & Grossman (1994), shown in Figure 3 as triangles, yield an extinction of ~ 0.5 and 0.9 mag from the $B-V$ and $V-R$ indices, respectively. The redder indices $V-I$ and $V-J$ give 1.2 and 1.8 mag of extinction, respectively. Thus V819 Tau also shows a trend similar to LkCa 7 in that the derived extinction values increase with wavelengths.

To examine whether this is a common property among WTTSs, we calculated the extinction by comparing the $B-V$, $V-R$, $V-I$, and $V-J$ color indices with those of main-sequence stars (KH) for K7–M1 WTTS in Taurus, for which the photometric data exists. Adopting the spectral types in KH and a standard reddening law, Figure 4 illustrates the results of correcting for reddening using the $V-R$ color. The WTTSs show a systematic trend toward redder colors with increasing wavelength of the color index, in addition to substantial scatter. This systematic trend will result in larger estimated extinctions with increasing wavelength of the color index adopted.

Several sources of the color anomalies have been considered:

Errors in the color calibrations—.This seems unlikely, since the mean relations from various sources agree reasonably well. As a check, in the lower panel of Figure 4 we show the color differences for the dwarf star Gl 913 (assuming no reddening), which we also use as a template star; there is no tendency toward the same trend as for the WTTSs.

Gravity effects that result in different colors than main-sequence stars.—To investigate this, we compared the near-infrared colors with those of giants (Bell & Gustafsson 1989; Amado & Byrne 1996) and found that giants have redder $V-I$ and $V-J$ indices by less than 0.1 mag. This should be an upper limit to the effect, since the gravities of WTTSs are intermediate between dwarfs and giants. To emphasize this point, the $B-V$ versus $V-R$ diagram (Fig. 3) suggests that WTTSs lie closer to the main sequence than the giant locus. Gravity effects appear to be much smaller than needed to account for the differences seen in Figure 4.

Errors in spectral typing.—Using the mean relations in KH, we find that changing the spectral type from K7 to M1

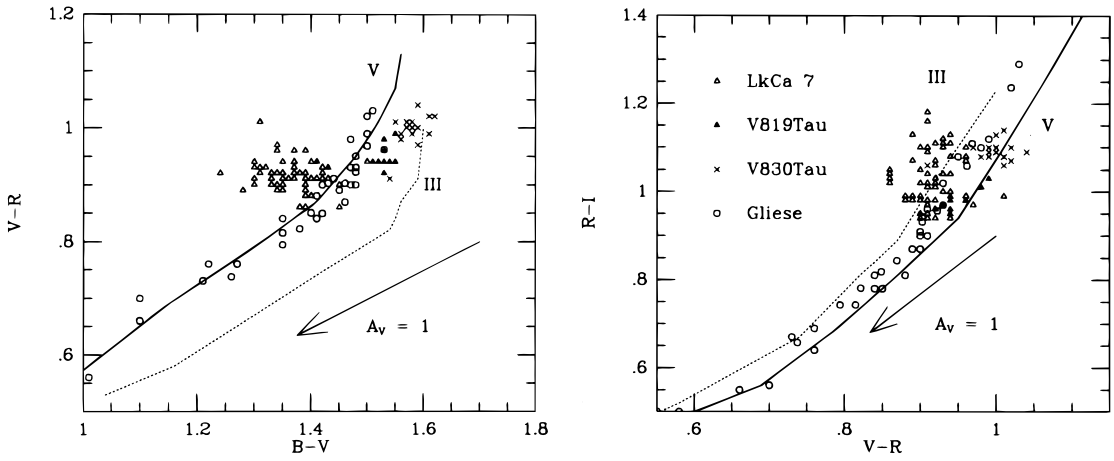

FIG. 3.—Colors of WTTSs of spectral type K7–M0 compared with colors of standard dwarfs and giants. The mean curves for luminosity class III and V are taken from Johnson (1966) transformed to the Cousins photometric system using the relations in Bessell (1979). Open circles are colors of sample nearby dwarf stars taken from Bessell (1990) and from Weis (1993); the latter colors in the Kron system were transformed to the Cousins system using the relations in Bessell & Weis (1987). The photometry of the WTTSs is taken from the catalog of Herbst et al. (1994); the scatter in the points indicates the level of variability in these stars.

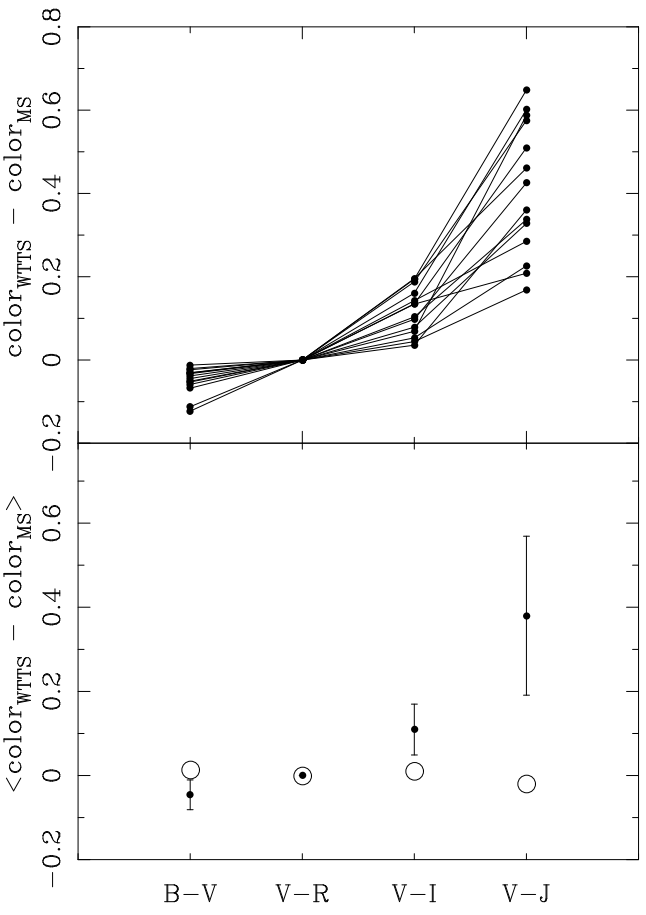

FIG. 4.—*Top*: The color anomalies of a number of K7–M1 WTTSs for different indices. The photometric data are from Kenyon & Hartmann (1995). The anomalies are calculated as the difference between the color indices of the WTTSs and a main-sequence star of similar spectral type, after dereddening the WTTSs with respect to their $V-R$ color. The stars included are LkCa 3, LkCa 4, LkCa 7, HBC 376, HBC 427, L1551-51, L1551-55, V819 Tau, V826 Tau, V827 Tau, V830 Tau, V836 Tau, VY Tau, and IW Tau. *Bottom*: The mean values. The circles show the color anomalies for the dwarf star Gl 913 (spectral type M0.5) taken from Weis (1993) and Leggett & Hawkins (1988).

reduces the $V-I$ and $V-J$ excesses by only ~ 0.13 and 0.21 mag, respectively. This is a fairly large change in spectral type, given the corresponding change in TiO band strengths, and so this also seems unlikely to account for most of the observed color anomalies.

Anomalous extinction.—In principle, an extinction law that is more gray than the standard law (i.e., a larger $R_V = A_V/E_{B-V}$) would yield a larger E_{V-J} for a given $B-V$ excess, and such extinction laws have been found in some star-forming regions. However, Kenyon, Dobrzyka, & Hartmann (1994) studied the extinction law in Taurus using background stars and found it to be similar to the standard extinction relation. Moreover, reasonable gray extinction laws do not seem to be capable of accounting for most of the observed effect; using the tabulation of Mathis (1990), changing the extinction law to an extreme value of $R_V = 5$ would result in $\Delta E_{V-J} = 1.16 E_{B-V}$; thus, for most of our program stars the change in $V-J$ colors would be about 0.3 mag.

Binary companions.— Cool stellar companions are very likely to have a substantial effect on the colors of some WTTSs, especially since these stars may be preferentially binary (see, e.g., Mathieu 1994). As an extreme example, the speckle photometry of LkCa 7 indicates that the secondary is about 0.6 mag fainter than the primary in the K band (Leinert et al. 1993). A fainter companion is probably cooler, and therefore will contribute more in the near-infrared than in the optical; the result will be an increasingly later spectral type, or redder colors, with increasing wavelength. It seems unlikely, however, that companion stars can account for the color anomalies of all of the stars shown in Figure 4.

Spots.— Photometric monitoring of WTTSs has shown periodic variations in brightness that have been attributed to spots rotating across the visible stellar surface (see, e.g., Bouvier et al. 1993, 1995; Herbst et al. 1994). In principle, cool spots can account qualitatively for the observed trend in the color anomalies; at short wavelengths, the spot is nearly black, and so one only observes the hotter stellar photosphere, whereas at longer wavelengths both spot and photosphere contribute. This would suppress the V-band flux of the star relative to I- and J-band fluxes, while at the same time the $B-V$ color would remain relatively blue.

To provide a quantitative estimate of the effects of spots, we calculated color indices for a K7 star with a spot having colors from M2 to M6 photospheres. The colors were assumed to be the same as for main-sequence stars and were taken from KH. We calculated the contribution to the emission by the spot from the fractional spot size and the effective temperatures of the stellar photosphere and the spot. We found that a spot with the same color as an M4 star provided the largest color anomaly in $V-J$, and a coverage of 50% of the stellar visible hemisphere was needed to get similar excesses as the mean values shown in Figure 4; to account for the stars with the reddest color indices, fractional sizes of more than 70% are needed. The periodic modulations of WTTS light curves indicate smaller spot sizes of the order of 20%, although higher values are found for some stars (Bouvier et al. 1993, 1995; Herbst et al. 1994). However, large axisymmetric spots, which could not be traced from brightness modulations, should be able to significantly affect the star's color. Indications of such polar spots are provided by Doppler imaging of WTTSs in, for instance, Hatzes (1995), for the WTTS V410 Tau, and Joncour, Bertout, & Bouvier (1994), for the WTTS HDE 283572. Thus, even if cool spots may not be responsible for all color anomalies of the WTTSs, they certainly account for some fraction of it.[5]

Strassmeier, Welty, & Rice (1994) and Rice & Strassmeier (1996) have suggested that V410 Tau has hotter "plage" regions on its surface in addition to dark spots (see Hatzes 1995 for a differing view). If indeed there are both hot and dark spots on WTTSs, it may be possible to explain the color anomalies of the WTTSs, although a convincing demonstration will require careful analysis of colors, variation of spectral type with wavelength, Doppler imaging, etc.

In this paper we take the view that the optical spectral types given in the literature are closely related to the optical colors; thus, we use $V-R$ (which usually agrees fairly well with $B-V$) to deredden the template stars, in particular

[5] High-resolution echelle spectrograms of LkCa 7 and DN Tau reveal, from the TiO bands in the spectral region 6185–7800 Å, that both stars show later spectral types (by three subclasses) at longer wavelengths (J. Muzerolle 1997, private communication).

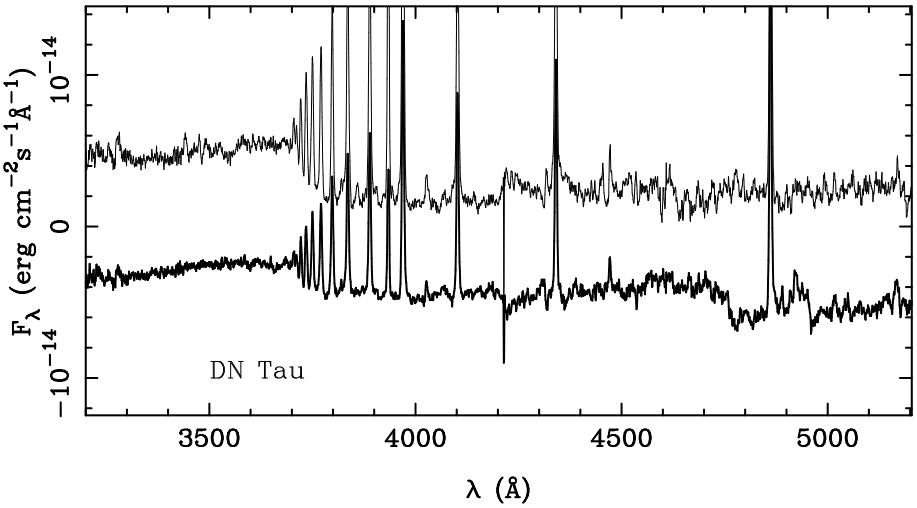

FIG. 5.—Excess spectrum of DN Tau with V819 Tau as template (*thick line*) (displaced downward by 8×10^{-15} flux units for clarity) and with Gl 913 as template (*thin line*).

V819 Tau. We also assume, following Kenyon et al. (1994), that the extinction law is normal in Taurus. Our assumptions imply that the redder colors of this star at longer wavelengths are due to a change in the average effective temperature at longer wavelengths, probably attributable in part to spots and possibly to an unresolved binary companion. We emphasize these assumptions, since the assumed extinction of the template star is propagated though the rest of the analysis.

3.4. *Choice of Template Stars*

The template stars we used were V819 Tau (~K7), Gl 913 (~M0–M0.5), and Gl 038 and Gl 051 for later spectral types. The choice of template was guided by spectral types from KH and by the goodness of fit. After subtraction of the dereddened, normalized template star the excess continuum should (presumably) only show very weak absorption structures, since we expect this emission to arise from regions with much higher effective temperature than the stellar photosphere.

For some stars we found that significant absorption features still remained after the subtraction of V819 Tau as a template; these features could be seen most strongly in some of the weakest emission stars. As an example, we show in Figure 5 the excess continuum of DN Tau (a star with low veiling) using V819 Tau as the template. The TiO structures at 4700–4850 Å are still present in the residual spectra. TiO bands are temperature sensitive, and the difference in the depths between the CTTS central star and the spectral template depends on spectral type mismatch as well as intrinsic variations in the line strength in one or both of the stars due to stellar spots (see Petrov et al. 1994). To test this, we used the main-sequence spectral standard Gl 913 with spectral type M0–M0.5 and zero extinction as a template. In Figure 5, the excess flux derived in this manner is shown. It is seen that the TiO features are now subtracted away much more efficiently, which implies that V819 Tau might have deeper features than expected from its spectral type alone (possibly caused by cool spots on the stellar surface). Conversely, the depth of the Ca I resonance line at 4226 Å seems to be larger in the Gliese star compared to V819 Tau, producing too high of an emission in the excess flux in that wavelengths region (see Fig. 5). Thatcher & Robinson (1993) found, in their high-dispersion spectra, that for late-type stars, the Ca I λ4226 line becomes much broader in active than in quiet stars, something that would affect the line depth in our lower resolution spectra. They also found that the Mg I λλ5167, 5172, 5183 lines were much less sensi-

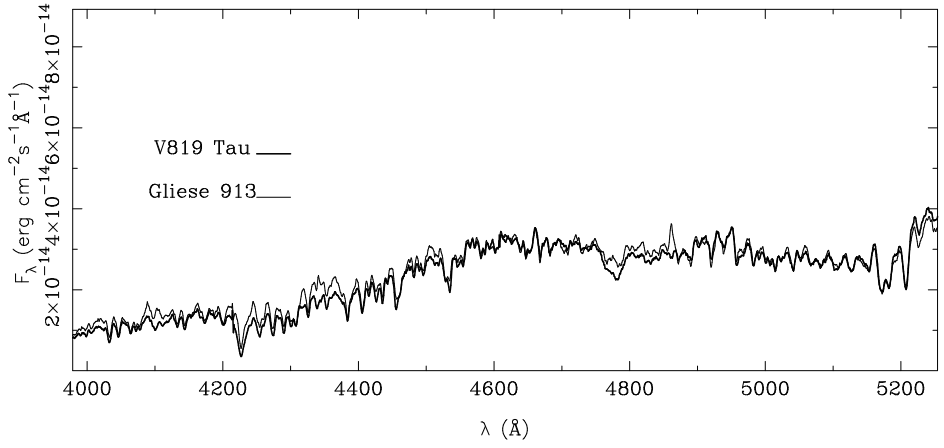

FIG. 6.—Comparison of the dereddened spectra of V819 Tau (*thick line*) and Gl 913 (*thin line*). Note the different line depth in the Ca I λ4226 line and in the TiO feature at ~4760 Å.

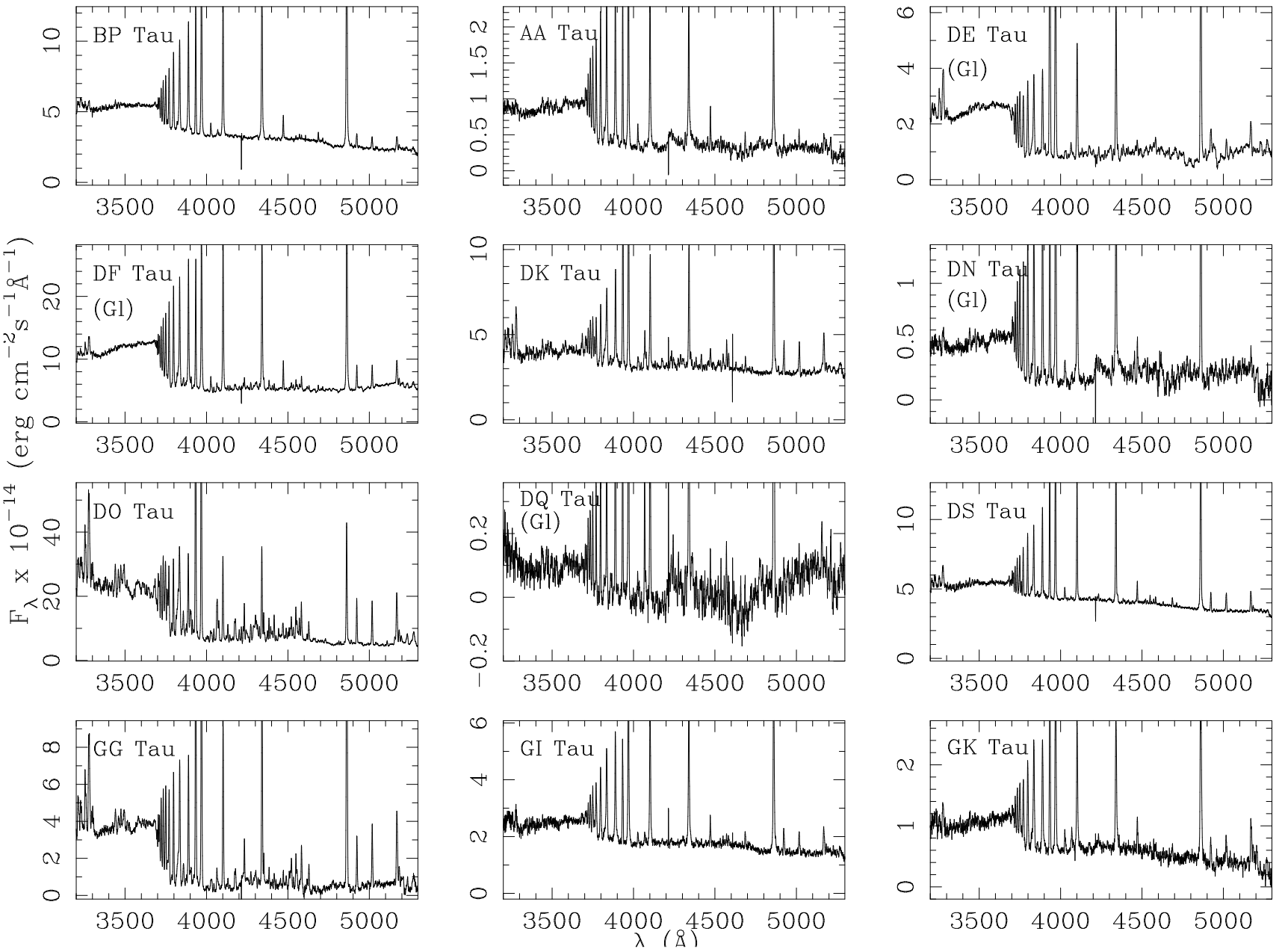

FIG. 7.—Extracted excess spectra of CTTSs. Note that the spectra are displayed with the same zero point but with different ranges in the flux scale. Excess spectra derived with Gliese stars as templates are marked with (Gl).

FIG. 7.—*Continued*

tive to stellar activity. We also note that the spectral features in the region close to 3550 Å become absorption features when a Gliese star is used as template but are almost absent if a WTTS is used instead. It is likely that the iron-line complex in this region comes more into emission for the more active WTTSs than for the Gliese stars and therefore suppresses the absorption. These spectral differences indicate an enhanced surface activity on V819 Tau. Since activity is related to the presence of stellar spots, this is in line with the discussion in § 3.3, that cool spots might be partly responsible to the color anomalies of WTTSs.

Figure 6 compares our flux-calibrated spectra of V819 Tau and Gl 913 (correcting the former for extinction). The comparison shows that the depths of both the TiO bands and the Ca I feature are different, while the other absorption features, notably the Mg I lines, are very similar. Fortunately, in spite of these discrepancies, using a WTTS or a Gliese (dwarf) star as template affects the derived total excess flux and the spectral slopes by only a small amount.

Note that, using our standard value of $A_V = 0.9$ mag for V819 Tau, our flux-calibrated spectra indicate similar optical colors for V819 Tau and GL 913, as would be expected given their similar spectral types. Had we adopted the extinction $A_V \sim 1.3$ mag for V819 Tau suggested by KH and HEG, our corrected spectrum of this weak-emission T Tauri star would be substantially bluer than that of Gl 913 (which is close enough to have negligible reddening); the implied color excess would be inconsistent with the small difference in spectral type.

4. RESULTS

4.1. *The Excess Flux Spectra*

In Figure 7, we present the excess flux spectra in the observed wavelength region for all the CTTSs in the sample for which we measured the veiling and were able to determine A_V. The excess spectra generally show that the Paschen continuum slightly decreases to longer wavelengths, together with a slightly decreasing Balmer continuum toward shorter wavelengths. Our Paschen continuum slopes are generally redder than those inferred by Hartigan et al. (1990, 1991), mostly because of the lower extinctions we use here. For example, our excess spectrum for BP Tau agrees very well with that of Hartigan et al. (1991) if we use LkCa 7 with $A_V = 0.7$ as a template (to match Hartigan et al.).

The subtraction of the stellar template from the observed spectra reveals many emission lines, seen all the way down to 3200 Å. Most of the emission lines are from Fe I and Fe II, with Fe II multiplets 1 and 6 in the wavelength region 3200 Å $< \lambda <$ 3300 Å and multiplets 27, 37 and 38 in the region 4200 Å $< \lambda <$ 4600 Å. For some stars, the iron lines in the region 4400 Å $< \lambda <$ 4600 Å almost give rise to a false continuum. The Ca II H and K lines, with Ca II H blended with Hϵ, are strong in most spectra, in some cases even stronger than the Balmer lines. In Table 2 we present values of the line fluxes and Balmer jumps of the excess emission spectra.

The excess continuum emission is thought to arise from the region of the accretion shock at the stellar surface (see § 3.1), while the emission lines are thought to arise in the freely infalling gas outside of the accretion shock, in the magnetosphere (Hartmann, Hewett, & Calvet 1994; Muzerolle, Calvet, & Hartmann 1997), based on the high-resolution profiles of these lines. The process or processes responsible for heating the magnetospheric gas and powering the line emission are uncertain, but some of the energy of accretion may be converted into magnetospheric heating, possibly by exciting MHD waves. To explore the possible relations between the continuum and the line-emitting regions, we searched for correlations between line strengths and properties of the Balmer and Paschen continua. We found that the line strength of the Ca II K line showed some correlation with the size of the Balmer jump, while none of the iron lines showed such correlation. As seen in Figure 8 (*top*), there is a strong correlation between the total observed excess flux and the strength of Hβ, i.e., the line flux after subtraction of the continuum. A similarly close relation was found for Hγ.

It is unlikely that the continuum and line-forming regions are the same because the continua appear to be at least partially optically thick (§ 4.2), which would make it difficult for the line strengths to be large relative to the continua. Nevertheless, the correlation suggests that the line emission is in some way powered by accretion. (The total energy emitted in the lines is small in comparison with that emitted in the continua.)

As shown in Figure 8 (*bottom*), the Balmer jump tends to decrease for higher degrees of veiling, although with some scatter for some stars. A similar relation was found by VBJ. Thus, either the emission region becomes more optically thick for higher accretion rates, or the Balmer and Paschen

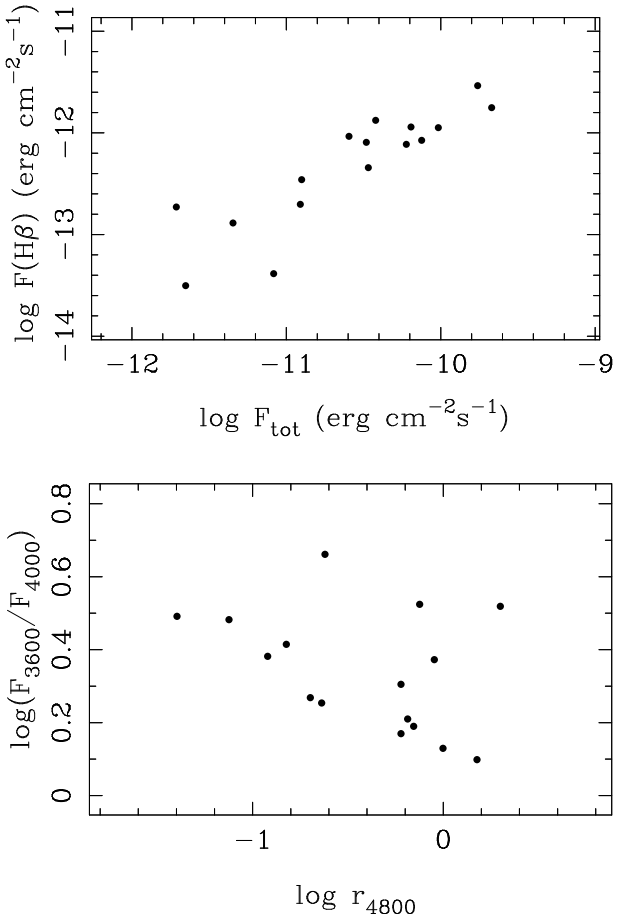

FIG. 8.—Correlation diagrams showing (*top*) the H_β line flux versus the total observed flux and (*bottom*) the size of the Balmer jump vs. the mean amount of veiling, measured in the spectral region 4500 Å $< \lambda <$ 5100 Å.

TABLE 2

FLUXES, BALMER JUMPS, AND VEILING OF THE EXCESS SPECTRA

Object	Hβ	Hγ	Hδ	Hε + Ca II H	Ca II K	Balmer Jump	F_{tot}(observed)	r	Template
BP Tau	15.9	10.9	7.7	10.0	6.1	1.7	8.3	0.65	V819 Tau
AA Tau	1.7	1.9	1.8	2.5	1.3	2.9	1.2	0.12	V819 Tau
DE Tau	7.9	4.5	3.2	7.1	8.9	3.3	3.3	0.75	Gl 038
DF Tau	29.4	20.8	17.4	20.4	12.6	2.5	16.7	0.90	Gl 038
DK Tau	9.9	7.0	5.0	9.1	7.6	1.4	7.7	0.96	V819 Tau
DN Tau	2.4	2.0	1.7	2.4	1.3	3.7	0.7	0.075	Gl 913
DO Tau[a].....	25.6	26.7	15.0	56.3	69.8	3.4	27.9	high	V819 Tau
DQ Tau	2.4	1.2	0.7	0.9	0.5	< 1.1	0.2	<0.02	Gl 913
DS Tau	12.1	9.0	5.9	8.6	6.3	1.3	9.8	1.5	V819 Tau
GG Tau	17.0	9.5	5.8	11.4	13.0	10.2	3.9	0.24	V819 Tau
GI Tau.....	6.0	5.2	4.4	5.4	2.5	1.5	4.4	0.60	V819 Tau
GK Tau	2.9	2.6	2.0	2.9	2.2	1.9	1.6	0.21	V819 Tau
GM Aur	12.3	6.5	4.2	3.8	1.8	1.8	3.3	0.23	V819 Tau
HN Tau	4.5	2.5	1.5	2.9	4.4	2.1	1.6	0.60	V819 Tau
IP Tau	0.9	0.8	0.6	1.0	0.6	3.5	0.3	0.15	Gl 913
UY Aur	17.8	15.6	10.5	13.8	9.4	1.6	12.5	0.70	V819 Tau
CY Tau	7.2	4.3	3.3	4.2	2.1	2.6	1.9	0.82	Gl 913

NOTE.—The Balmer jump is defined as the ratio between the fluxes at 3600 Å and 4000 Å. Line fluxes are continuum subtracted and given in units 10^{-13} ergs $s^{-1}cm^{-2}$ and the total observed fluxes, F_{tot}, in 10^{-11} ergs $s^{-1}cm^{-2}$. The veiling r is taken as the mean value in the spectral region 4500 Å $< \lambda <$ 5100 Å. The last column gives the template star used for the extraction.

[a] It is difficult to measure the high amount of veiling. The fluxes should be considered as lower limits.

continuum originate from different regions, providing a stronger Paschen continua at higher accretion rates. We also find that for higher emission in the Balmer continuum the Balmer jump decreases, which seems to suggest that for higher excess fluxes, the emission in the Paschen continuum increases faster than in the Balmer continuum.

4.2. *Accretion Luminosities*

To determine the total accretion luminosity, it is necessary to account for the excess emission outside of our wavelength range. This depends on the nature of the emission region where the mass flow settles on the stellar surface. In this work, we assume that the hot continuum comes from a region of constant temperature and density ("slab" model)—a condition certainly not expected in the shock region, where the radiation temperature ranges from close to 10^6 K to less than 10,000 K. We are presently developing a more refined model for this region, but since our purpose here is only to estimate the bolometric correction, a slab model should be sufficient. Slab models have previously been used for this purpose by others (Hartigan et al. 1991; VBJ).

The slab model is characterized by three parameters: temperature, density, and physical depth, or, equivalently, the optical depth at some fixed wavelength. Hydrogen and H^- are included as opacity sources. For each model, we solve the statistical equilibrium equations for an eight-level hydrogen atom, with the radiation field in the lines characterized by the static escape probability. The Lyman continuum is assumed in detailed balance, while the rest of the continua are characterized by radiation temperatures. H^- is assumed in LTE.

In the upper panel of Figure 9, we show the ratio log F_{3600}/log F_{4000} (i.e., the Balmer jump) plotted against the ratio log F_{4750}/log F_{4000}, which measures the slope of the Paschen continuum, for models with temperatures 6000, 8000, 10,000, and 20,000 K, and optical depths at the Balmer threshold, τ_{3640}, of 0.1, 1, and 10. These models are calculated for a hydrogen density of $n_H = 10^{14}$ cm^{-3}. The observed ratios, also shown in Figure 9, indicate high optical depths, $\tau_{3640} \sim 1$–10 and temperatures of $\sim 10^4$ K. This high value of the optical depth requires n_H to be $\geq 10^{13}$ cm^{-3} if the size of the emitting region is to be smaller than the stellar radius, which would be consistent with the value adopted for n_H. We note that these ratios are similar for $n_H \geq 10^{13}$ cm^{-3}, since the gas is essentially in LTE. These estimates of density and temperature are similar to those previously found by Hartigan et al. (1991) and VBJ.

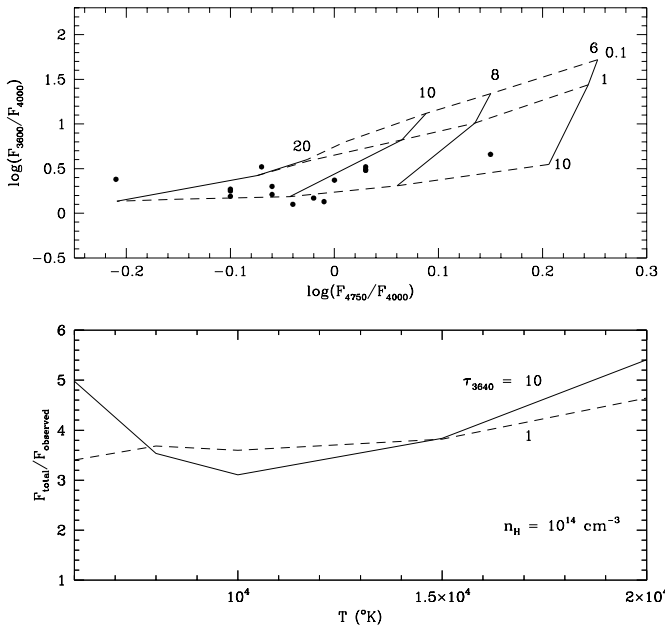

FIG. 9.—*Top*: Balmer jump vs. Paschen continuum slope for uniform isothermal slabs. Continuous lines join models with the same temperature, labeled by $T/10^3$. Dashed lines join models with the same optical depth at the Balmer threshold, τ_{3640}, labeled by the value of the optical depth. Balmer jumps and Paschen continuum slopes for the observed stars are also shown. *Bottom*: Ratio of the total flux emitted by the slab to the flux in the observed range as a function of temperature, shown for $\tau_{3640} = 1$ (*dashed line*) and 10 (*continuous line*). The models are calculated for $n_H = 10^{14}$ cm^{-3}.

We also compared the ratio $\log F_{3600}/\log F_{3400}$, which measures the slope of the Balmer continuum, with the observed values. We find that the observed slopes indicate lower values for the slab temperature than the Paschen continuum. This behavior may be due to several factors. As we indicated, the regions emitting the excess flux are expected to have a large range of temperatures, and their fluxes are not expected to be consistent with that of a single temperature slab. However, the Balmer continuum slope is measured at wavelengths that are very close to each other, with similar flux values, so the slope is very small and close to our calibration errors and subtraction procedure. We prefer to wait until we have more elaborate models for the emitting region and can compare the overall shape of the predicted fluxes with the observations to make more definite statements regarding the Balmer continuum.

The lower panel of Figure 9 shows the ratio of the total flux to the flux in the observed interval, 3200–5300 Å. For $T \sim 10^4$ K, the ratio is $\sim$3–3.5. The uncertainties in this modeling, both in terms of the observational data and the theoretical simplifications used, preclude any attempt to derive flux corrections for individual stars. We therefore have adopted a uniform factor of 3.5 to convert from our measured excess fluxes to the total excess luminosity.

4.3. *Mass Accretion Rates*

In the magnetospheric model, the luminosity released in the impact of the accretion flow can be derived from the energy equation as

$$L_{\rm acc} \simeq \frac{GM_* \dot{M}}{R_*}\left(1 - \frac{R_*}{R_{\rm in}}\right), \quad (8)$$

where M_* and R_* are the stellar mass and radius, and $R_{\rm in}$ is the inner radius of the accretion disk. The value for $R_{\rm in}$ is uncertain and depends on the details describing the process by which the disk flow couples to the stellar magnetic field (see, e.g., Ghosh & Lamb 1979a, 1979b; Wang 1995). Certainly $R_{\rm in}$ is less than the co-rotation radius, typically 5–6 R_*, to permit accretion down to the central star. In the following, we will adopt $R_{\rm in} = 5R_*$, i.e., $1 - R_*/R_{\rm in} = 0.8$, for all stars.

The observed luminosity also depends on the inclination of the star, a parameter known in only a few cases. Simple geometrical models for accretion rings for dipolar magnetospheres suggest that the ratio of the apparent to the true luminosity might vary by a factor of $\sim$2 for differing system inclinations. We ignore this factor in our results, since on average there should be no effect.

To obtain the stellar masses and radii, estimates of the stellar luminosities (without the excess component) as well as the effective temperatures are needed. For comparison, we calculated the stellar luminosities in two ways: (1) using the derived values of the normalization constants, C_1, from equations (4) or (5) together with the brightness of the template star; and (2) using the derived values of the interstellar extinction together with published J-band magnitudes (from KH) for each star. In the first method, we used V819 Tau, dereddened by 0.9 mag, as a template for all stars. As was mentioned in § 3.3, the difference in the achieved luminosities by using V819 Tau instead of Gliese stars, with more appropriate spectral types, is negligible. The luminosity of V819 Tau was estimated from its J magnitude together with the J-band bolometric correction given by KH. In Figure 10 the stellar luminosities, derived by the two methods, are plotted against each other, and it is seen that they agree fairly well. In order to avoid possible scatter induced by fitting the value of C_1, we decided to use the stellar luminosities derived from the J magnitude for the luminosity determinations. The spectral type conversion to effective temperature is from KH. The masses and radii were then derived from the evolutionary tracks by D'Antona & Mazzitelli (1994) using Alexander opacities and Canuto & Mazzitelli (CM) convection.

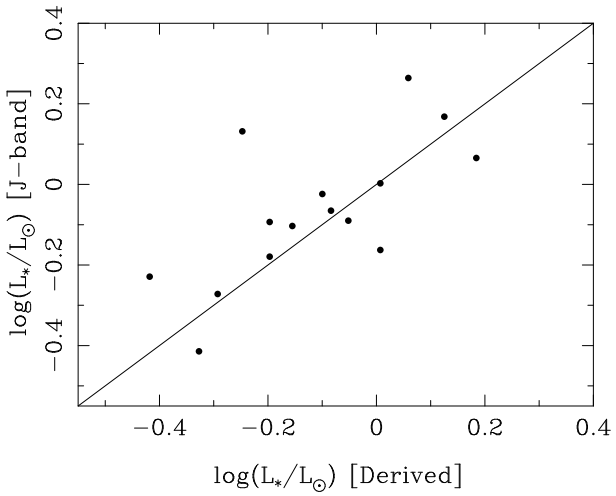

FIG. 10.—Comparison between stellar luminosities derived from J-band brightnesses ([J-band]) and from the blue spectra ([Derived]). See text for details.

In Table 3, we present the derived accretion rates together with the other stellar parameters for the CTTSs in our sample. The accretion rates range over nearly 2 orders of magnitude. Note that we were not able to determine extinctions for the strongest emission stars in our sample—DG Tau, RW Aur, CW Tau, and DR Tau—so that high accretion rates must be underrepresented in our final sample.

Six of the stars shown in Table 3 (DF Tau, DK Tau, GG Rau, DL Tau, DQ Tau, and UY Aur) are binaries, known both from speckle interferometry in K and from spectroscopy (Leinert et al. 1993; Mathieu et al. 1997; Simon et al. 1992). For most of these stars, the K-band brightnesses of the secondary components are low, or the angular separations for the systems are rather wide. However, DF Tau and DQ Tau are both close binaries with angular separations of less than 0.″1. Thiébaut et al. (1995) resolved the DF Tau system by speckle interferometry and managed to estimate spectral energy distribution models including the two components. It appears, from these models, that the T Tauri type component (with disk) should dominate the emission at the wavelengths covered by our observations. Still, we note that the stellar luminosity for DF Tau seems to be quite high for its spectral type and note that possibly a correction for the secondary component should be made. This would also influence the determined accretion rate, which depends on the mass and radius of the star. DQ Tau was found to be a spectroscopic binary by Mathieu et al. (1997), surrounded by a circumbinary disk. the stellar parameters and accretion rate of DQ Tau (Table 3) should also be corrected for this. In general, it is difficult to account for binarity when deriving the stellar parameters, since nor-

TABLE 3

STELLAR PARAMETERS FOR THE CTTSs

Object	L_* ($L_\odot$)	log (age) (yr)	M ($M_\odot$)	R_* ($R_\odot$)	A_V	L_{acc} ($L_\odot$)	$\dot{M}$ ($\times 10^{-7}$ $M_\odot$ yr^{-1})
BP Tau	0.925	5.79	0.490	1.99	0.51	0.179	0.288
DN Tau	0.87	5.69	0.382	2.09	0.25	0.016	0.035
DF Tau	1.97	3.59	0.27	3.37	0.45	0.358	1.769
DE Tau	0.87	5.01	0.259	2.45	0.62	0.071	0.264
DK Tau	1.45	5.56	0.431	2.49	1.42	0.166	0.379
AA Tau	0.71	5.98	0.530	1.74	0.74	0.025	0.033
GG Tau	1.25	5.63	0.442	2.31	0.60	0.084	0.175
DQ Tau	0.635	5.88	0.439	1.785	0.71	0.004	0.006
HN Tau	0.19	7.49	0.81	0.76	0.65	0.035	0.013
GM Aur	0.74	5.95	0.524	1.78	0.31	0.071	0.096
UY Aur	1.585	5.52	0.421	2.60	1.26	0.268	0.656
GI Tau.....	0.85	6.09	0.668	1.735	1.34	0.094	0.096
DS Tau	0.57	6.58	0.870	1.36	0.34	0.209	0.129
IP Tau	0.41	6.23	0.522	1.44	0.32	0.007	0.008
GK Tau	1.08	5.70	0.461	2.15	0.94	0.035	0.064
DO Tau[a].....	1.01	5.625	0.369	2.25	2.27	0.600	1.442
CY Tau	0.46	6.32	0.424	1.63	0.32	0.041	0.075

[a] It is difficult to measure the high amount of veiling. The values are calculated for the presented A_V, which should be considered as a minimum value.

mally the orbital elements of the systems are not well known, and the properties of the gas flow between the disk and the components are uncertain (see, however, Artymowicz & Lubow 1996).

5. DISCUSSION

5.1. *Comparison with Other Work*

Hartigan et al. (1991), VBJ, and HEG have estimated accretion rates for T Tauri stars (TTSs) in the Taurus-Auriga star-forming region; HEG and Hartigan et al. (1991) used echelle spectra (Hartigan et al. 1991 also used roughly simultaneous spectrophotometry with lower dispersion) to measure the veiling, and VBJ used low-dispersion blue spectra. As discussed in § 1, their results differ systematically by almost 1 order of magnitude. Our results (Table 3) are generally much closer to the values presented by VBJ than to HEG. Here we discuss the reasons that different results have been obtained.

In Figure 11, we compare our derived accretion luminosities with those of VBJ and HEG for stars in common. The luminosities of HEG are higher than ours typically by a factor of 5–6, while the values of VBJ are in better agreement. A certain amount of time variability in the accretion luminosities is expected, but such variations can hardly be responsible for any large systematic differences. This conclusion is supported by Figure 12, which compares our veiling values, r_{4800}, with those found by HEG at 5700 Å. The correlation is good, which suggests that time-variability cannot be responsible for the disagreement with HEG nor can systematic differences in estimated optical veilings resulting from the different methods employed.

HEG assumed that the hot excess emission arises in a boundary layer and that one-half of this emission is absorbed by the central star, since it subtends approximately one-half of the solid angle into which the boundary layer may radiate. At the same time, they assume that the disk does not block any of the photospheric emission. We assume that the hot emission arises in the accretion shock region; all of the excess heat generated by accretion is radiated out of the star. These differing assumptions account for an immediate factor of 2 between our results and those of HEG.

It appears that most of the rest of the discrepancy in accretion luminosities with HEG arise from the differing extinctions adopted. Figure 13 shows that the A_V values derived by HEG are often 0.6–1.0 mag larger than ours. Although part of this discrepancy might be due to differ-

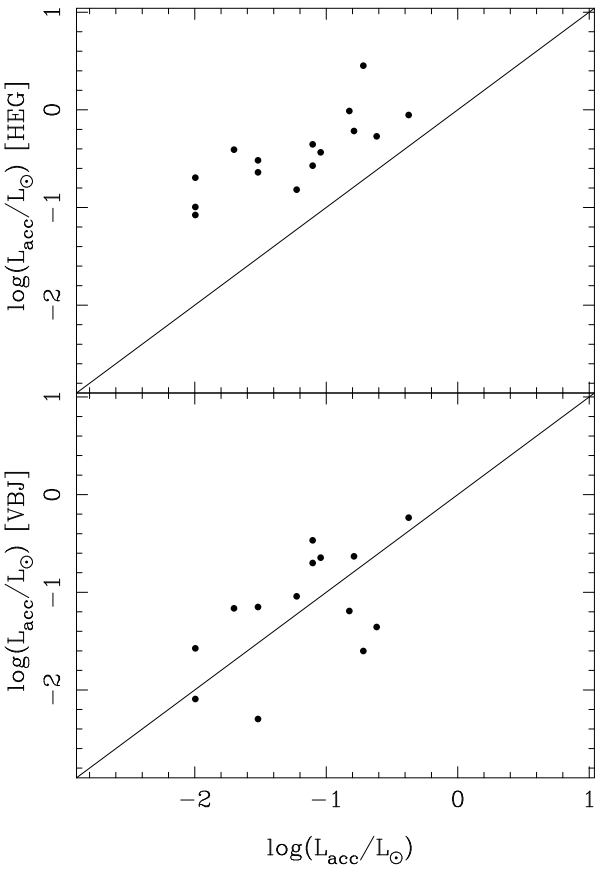

FIG. 11.—Comparison of accretion luminosities from this work and with those of (*top*) Hartigan et al. (1995) and (*bottom*) Valenti et al. (1993).

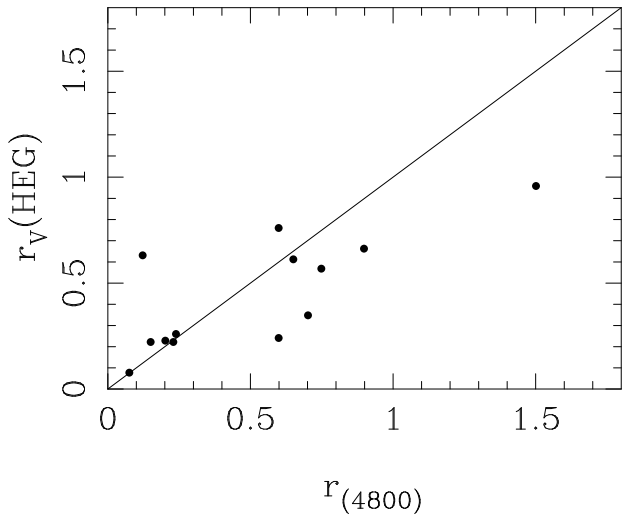

FIG. 12.—Comparison of the veiling r_{4800}, taken as the mean value in the spectral region 4500 Å $< \lambda <$ 5100 Å, with the veiling in the V band from Hartigan et al. (1995).

ences in the estimated effect of the hot excess continuum on system colors, it appears that most of the discrepancy is due to the color anomalies discussed in § 3.2. For example, in the weakly accreting M0 star DN Tau, HEG estimate A_V to be $\sim$1.1, whereas KH estimate A_V to be $\sim$0.5, and we adopt $A_V \sim 0.2$. Our estimated extinction near zero for this star is consistent with its mean $B-V$ and $V-R$ colors from KH. If we use instead $V-I$ or $V-J$ colors, we get $A_V \sim 0.3$ and $A_V \sim 0.65$, respectively. If we adopt the HEG estimate for DN Tau, then the true stellar $B-V \sim 1.1$, which would be more consistent with a K4–K5 star than with an M0 spectral type. HEG determine the extinction from the $V-J$ colors, assuming the intrinsic colors to be that of a main-sequence star. However, as the $V-J$ colors of a K7 T TTS stellar component is 0.3–0.9 mag redder than a normal star, the A_V gets overestimated by 0.4–1.2 mag, which is similar to the difference between our extinction values and those of HEG.

HEG used two methods to estimate L_{acc}: (1) from the veiling in the V band, the bolometric corrections of the stellar and excess components, and the stellar brightness (derived from J-band magnitudes); and (2) from the veiling and brightness in V together with the bolometric correction for the excess component. For method (2), it is evident that the difference in extinctions adopted will produce a corresponding difference in accretion luminosity estimates.

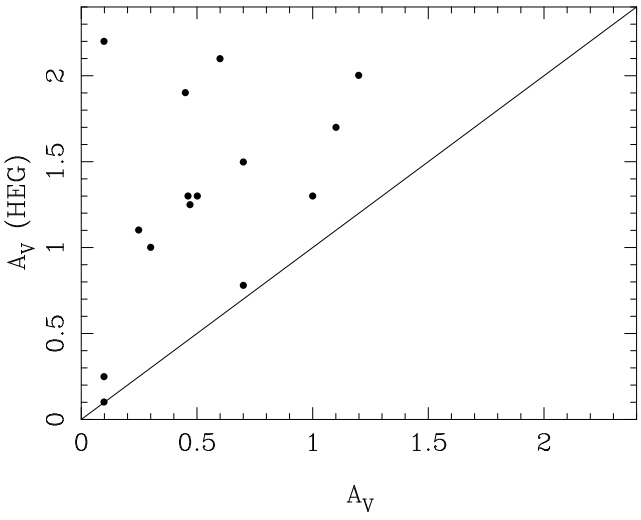

FIG. 13.—Comparison of values for the interstellar extinction from this work and from Hartigan et al. (1995).

Method (1) uses the optical r value to obtain the ratio of veiling to stellar continuum emission at V, which is reddening independent. Then, using a bolometric correction for the star at V and a near-infrared stellar luminosity, one can infer the intrinsic brightness of the star at V, and hence, from r, determine the intrinsic brightness of the hot continuum. Although this method appears to be formally independent of the extinction used, it does presume that the relationship between the stellar luminosity measured in the near-infrared and the stellar V magnitude is known; this effectively means that the $V-J$ colors of the template star or standard stars are known. As discussed above, color anomalies exist in most WTTSs that cause their $V-J$ colors to depart from those of main-sequence stars. Thus, method (1) implies that the standard star's brightness at V relative to J is intrinsically much brighter than we have assumed here, which increases the accretion luminosity (by factors comparable to the difference in extinction at V). An alternative way of putting this is to note that (as HEG pointed out) this method is very sensitive to the assumed stellar spectral type; in effect, the color anomalies imply that the spectral types are generally systematically later at longer wavelengths, perhaps owing to cooler companions, starspots, or both. As we have shown in § 3.2, the color anomalies will result in the $B-V$ and $V-R$ colors being much too blue for the extinctions of HEG, so we do not favor the high extinctions.

The minor discrepancies still remaining between our results and those of HEG are probably related to their adopted BC_V for the excess component. The value of -0.4 that they use is appropriate for a 10,000 K star, but since the emission region is certainly not optically thick (see § 4.2), this correction will overestimate the luminosity. We estimated the value of BC_V for the excess flux both from the model presented in § 4.2 and from the extracted spectra. By considering different temperatures, densities, and Balmer optical depths, as discussed in § 4.2, we found from the model that BC_V could vary by as much as 1 mag; the same result was found from our excess spectra by comparing an estimated V magnitude with the derived total flux. The scatter in BC_V is mainly due to the strength of the Balmer jump, and since we measure directly a large part of the emission shortward and longward of the Balmer jump, the choice of bolometric correction for our wavelengths interval is less crucial.

VBJ also present slightly higher values of the extinction than ours, many of which were taken from the literature. These differences account pretty well for the small discrepancies between their values and our values of the accretion luminosity.

Our mass accretion rates differ from those of HEG not only because of the difference in accretion luminosities but because of additional factors as well. HEG assume that the hot continuum emission comes from a boundary layer and so represents one-half of the accretion luminosity, while we assume from the magnetosphere model that this fraction is actually closer to 80%. In addition, the smaller extinctions we adopt result in smaller stellar radii, which increases the

value of M_*/R_* and thus also decreases the mass accretion rate for a given luminosity. All of these factors—the factor of 2 for the absorption of boundary layer emission, the factor of $\sim$2–3 due to differing accretion luminosities (differing extinctions), the factor of 1.6 between the dissipation in boundary layers and magnetospheres, and the reduction in stellar radius—all work in the same direction and result in $\sim$1 order of magnitude lower accretion rates in the present work. As pointed out in the beginning of this section, the discrepancy with the mass-accretion rates of VBJ is smaller; although we have somewhat smaller extinctions, the discrepancy is not as large as with HEG, and the factor of 1.6 due to magnetospheric rather than boundary layer dissipation is offset by the fact that VBJ use other evolutionary tracks than we do and therefore get systematically higher values for M_*/R_*.

In Table 4 we summarize the sources responsible for the differences between our accretion rates and those of VBJ and HEG. This table is intended to clarify the sources for the systematic differences and gives only typical values that differ for different stars.

It is difficult to estimate absolute errors in our estimated accretion luminosities. Given the color anomalies of TTSs discussed in the previous section, it is difficult to determine extinctions more precisely than $A_V \sim 0.3$–0.5 mag, which would translate into errors in accretion luminosities of factors of $\sim$1.5–2. The bolometric corrections used are also uncertain; we estimate this uncertainty as being yet another factor of 1.5, although this should be investigated using observations over a broader wavelength region, especially to the ultraviolet. The apparent accretion luminosity might also depend upon the inclination of the star, since it is unlikely that the accreting region is uniformly spread over the stellar surface; simple calculations suggest that this might correspond to another factor of 1.5 variation. Finally, there are uncertainties due to time-variability, either because of intrinsic variations in accretion rate or because of rotational modulation of the nonaxisymmetric magnetosphere, which might add another factor of 2 uncertainty (presumably this can be reduced with observations averaging over a wider time baseline). Putting all of these errors together in quadrature, we suggest typical errors of $\sim$3 in L_{acc} for an individual star and a comparable error in the mass accretion rates. The magnitude of any systematic errors is difficult to ascertain; such systematic effects would arise mostly from the color anomalies and bolometric corrections, which suggests that systematic effects might be as large as a factor of 2–3. Simultaneous observations over a wider range of wavelengths, especially at ultraviolet wavelengths, are needed to further improve the estimates.

TABLE 4

SOURCES OF DISCREPANCIES IN ACCRETION RATES

CAUSE	$\dot{M}/\dot{M}$ VBJ	$\dot{M}/\dot{M}$ HEG
Magnetospheric geometry.....	1/1.6	1/1.6
Interstellar reddening[a]	1/1.5	1/3
Radiative transfer	...	1/2
Distance.....	1/1.3	...
Evolutionary tracks[b].....	2.5/1	...
Bolometric corrections[c]	$\sim$1:	$\sim$1/1.5:
Total.....	$\sim$0.8	$\sim$0.07

[a] Includes secondary effects caused by different reddenings, such as stellar radii and masses.

[b] Giving different M/R.

[c] This factor may have vastly different values for different stars.

5.2. L_{acc} *versus U-band Brightness*

We next investigate the possibility of estimating T Tauri accretion luminosities from broadband photometry. A photometric calibration would be highly desirable; the relative ease of obtaining calibrated photometry versus calibrated spectra would permit rapid analysis of large samples of stars, and repeat observations to reduce the errors from time variability would be much more feasible.

The excess emission dominates the observed flux at wavelengths shorter than 4500 Å, where the stellar flux component drops significantly, which indicates that a relation between U-band photometric brightness and the excess luminosity could be expected. Since there exist a large amount of photometric data and new data can easily be collected even with small telescopes, such a relation would provide an opportunity to estimate accretion luminosities, and therefore accretion rates, for big samples of T Tauri stars.

To investigate this, we compared the dereddened U-band luminosity of the stars, L_U, after subtraction of the U-band emission from the stellar photosphere, with L_{acc}. The U magnitudes were adopted in two ways: (1) synthesizing a U magnitude from our observed spectra (shown in Fig. 1), where the response curve for the U filter was taken from Bessell (1990); and (2) taking mean values of published photometric observations (adopted from KH), where the luminosity were calculated from the U bandwidth (680 Å) and zero magnitude flux (4.27×10^{-9} ergs s^{-1} cm^{-2} Å^{-1}) given by Allen (1973).

Using the synthesized U magnitudes has the advantage of providing simultaneous values of L_U and L_{acc}, which minimizes scatter from intrinsic brightness variations of the star. On the other hand, the photometric data provide values for the mean U-band brightnesses. Comparing the two types of U magnitudes showed that the mean deviation was 0.45 mag, an amount expected from intrinsic variability alone. To minimize the scatter in the data, we decided to use the synthetic U-band magnitudes for the calibration.

The U magnitude was then dereddened by our derived extinction values (Table 3). To estimate the stellar contribution we used two methods, for comparison: (1) from the I-band brightness, then using the bolometric correction for the I band (Bessell 1995) together with the color of a main-sequence star (KH) of similar spectral type; and (2) from our derived values in Table 3. The J band may provide a more reliable estimate of the stellar brightness than the I band (see, however, the discussion of the color anomalies in § 3.3), but, in terms of large samples of stars, the I magnitudes are normally easier to obtain. It turned out that the differences in the L_U values caused by using these two methods were small, apparently because the contribution from a K5–M2 star is low in the U band. More important is the uncertainty in the bolometric correction for the stellar emission, as discussed in § 3.3, and how much the excess continuum contributes in I.

Figure 14 shows that L_U is highly correlated with L_{acc}. The relation is so well constrained that it can be used as a calibration between dereddened U magnitudes and total accretion luminosities. A least-squares fit of the data, which

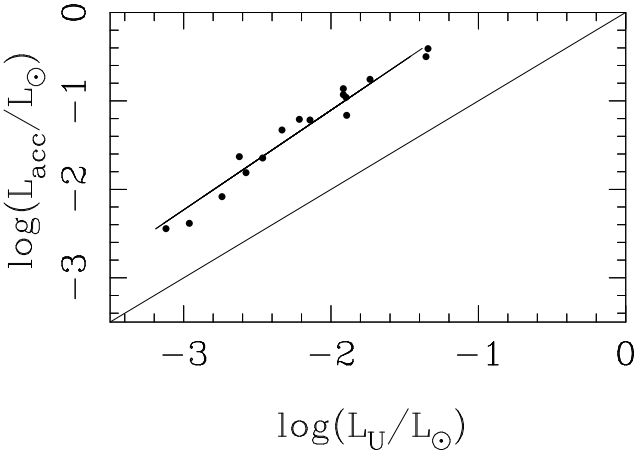

FIG. 14.—Relation between the dereddened U-band brightness and the total excess luminosity (from Table 2). The stellar contribution was estimated from I-band brightnesses.

accounts for individual errors in two dimensions, gives the relation

$$\log (L_{\rm acc}/L_\odot) = 1.09^{+0.04}_{-0.18} \log (L_U/L_\odot) + 0.98^{+0.02}_{-0.07} . \quad (9)$$

The individual errors in L_U were adopted from the scatter in the U magnitude given in KH and in $L_{\rm acc}$ by assuming a 15% uncertainty from our method. However, the errors shown for the fit are dominated by the uncertainty in estimating the contribution of the stellar component. Equation (9) implies a bolometric correction for the U-band luminosity ($L_{\rm acc}/L_U$) of $\sim$9.2–9.5. For comparison, the slab model, presented in § 4.2, indicates values for the correction in the range 4–11, with the higher values found for larger optical depth at the Balmer threshold.

These results indicate that, if the extinction can somehow be estimated and the stellar spectral type is known, good accretion luminosities can be derived from broadband photometry. Another implication of Figure 14 is that small details of the subtraction of the stellar spectrum do not matter much. For many CTTSs, the Balmer continuum is a major fraction of the total accretion luminosity, and it is much brighter than the stellar photosphere in the UV. In turn, this indicates that our imperfect subtraction of the stellar spectra in the Paschen continua for some CTTSs does not introduce major uncertainties in our results. Also, the fit given in equation (9) shows that the $L_{\rm acc}$ versus L_U relation is linear, which implies that, independent of the accretion rate, much of the emission emerges in the Balmer continua. What this does mean, however, is that the extinction correction is important.

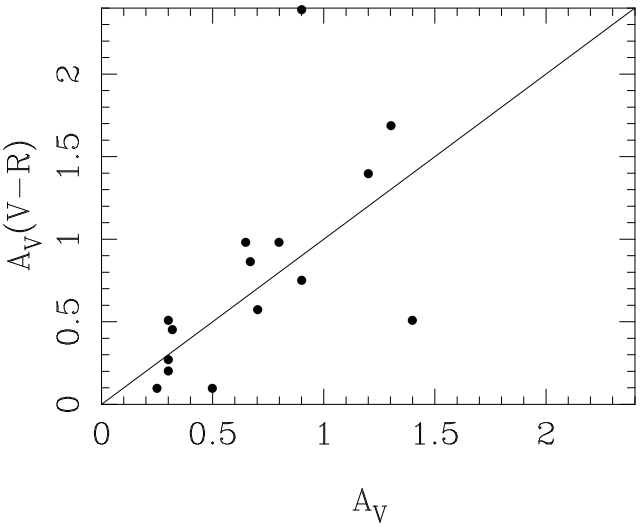

FIG. 15.—Comparison between interstellar extinctions determined from the $V-R$ color index and extinctions taken from Table 3.

We next explored the best way to estimate good values of A_V for veiled TTSs from broadband photometry. Since the $B-V$ color index is likely to underestimate the extinction of veiled stars by a significant amount (see also the discussion in HEG), we investigated whether other color indices would give more reliable values of A_V. To see how the veiling influences the extinction determination, it is informative to look at the expression for a color index (for colors j and i) of a reddened, veiled star:

$$(m_j - m_i)_0 - (m_j - m_i)_{\rm obj} = \frac{1}{R_{ji}} A_V + \log \left(\frac{1 + r_j}{1 + r_i} \right), \quad (10)$$

where m is the magnitude, 0 and obj denote the unreddened comparison star and the veiled object, and R_{ji} is given by the extinction law. The last term on the right-hand side gives the correction for veiling; in the case of no veiling ($r_i = r_j = 0$), equation (10) reduces to the standard expression for A_V for a nonveiled star. Note that this is also true if the veiling is the same at the two wavelengths (i.e., $r_i = r_j$). Therefore, it is not only the amount of veiling that affects A_V estimates but also the ratio between the amount of veiling at the wavelengths of the color index. For the B and V bands, the values of r differ significantly, but at longer wavelength regions, where both the spectral energy distributions of the stellar and the excess fluxes are rather flat, the relative veiling is nearly constant. Indeed, Hartigan et al. (1991) show, from their red echelle spectra, that r changes only slowly or not at all between the V and R spectral regions. Figure 15 shows comparisons between the broadband estimates of the extinction, $A_{V(\rm broad)}$ (photometric data from KH), with the values of A_V presented in Table 3. In Figure 15 we assumed $r_V = r_R$ when deriving $A_{V(\rm broad)}$, i.e., we ignored the effect of veiling. These A_Vs agree well with those from Table 3, most likely because $r_V = r_R$ is not a bad assumption (as discussed above). Therefore, we conclude that $V-R$ provides a good index for estimating A_Vs for moderately veiled stars. This method is unlikely to work for highly veiled stars, since the hot continuum is, at least, bluer than the stellar photosphere by an unknown amount. For most CTTSs, $V-I$ does not work as well as $V-R$ for two reasons: the wavelength difference between V and I is large so that r might change significantly and, as was discussed in § 3.3, $V-I$ is not suitable for measuring A_V both because of its sensitivity to the spectral type and because of the color anomaly.

6. SUMMARY

We have presented spectrophotometric observations of 29 classical T Tauri stars in the Taurus-Auriga star-forming region. The spectra cover a wavelength range of 5400 Å to near the atmospheric cutoff at 3200 Å. For 17 of the stars, which show modest amounts of veiling, we derived accretion rates and values for the interstellar extinction. The accretion rates range typically between 10^{-9} and $10^{-7}\ M_\odot$

yr^{-1}. To derive the correct spectral energy distribution of the excess emission, we note that the choice of the template star, as well as its extinction, is crucial. In particular, we found that the stellar colors of weak-line T Tauri stars are redder in the near-infrared than main-sequence stars of similar spectral types. These color anomalies affect estimates of the interstellar extinction as well as estimates of the bolometric correction. The estimated accretion luminosities and mass accretion rates also depend in a significant way on the assumed geometry of accretion; we adopt the magnetospheric accretion model, which results in lower accretion rates than would be derived in the boundary layer picture.

We found a very tight correlation between dereddened U-band and total accretion luminosities and argue that deriving the interstellar extinction of moderately to lightly veiled stars from broadband photometry is best done by using the $V-R$ index. In particular, if broadband measurements can be combined with low-dispersion spectra, reasonably accurate accretion luminosities can be determined relatively easily for large samples of stars. However, it would be necessary to eliminate heavily veiled, strongly accreting stars from such an analysis, since our methods are not suited to cases in which the hot continuum luminosity is much greater than that of the stellar photosphere.

Our measured accretion luminosities, plus the suggested U-band scaling, provide a starting point for estimating mass accretion rates for significant samples of T Tauri stars, which will result in additional constraints on disk evolution, as will be discussed in a forthcoming paper (Hartmann et al. 1998). Further detailed investigations aimed at understanding the colors and extinctions of T Tauri stars, as well as observations of hot continuum emission at ultraviolet wavelengths, are essential to reducing the systematic errors present in current estimates of disk accretion rates.

We would like to acknowledge the assistance of Craig Foltz in preparation for observing with the Multiple Mirror Telescope Spectrograph and Carol Heller in obtaining the observations. We wish to thank the referee, Pat Hartigan, for his helpful comments that improved the clarity of this paper. E. G. thanks the Swedish Natural Science Research Council for financial support. C. B. acknowledges support from the Predoctoral Fellow Program of the Smithsonian Institution and financial support from the Consejo Nacional de Investigaciones Científicas y Tecnológicas (CONICIT, Venezuela). This research was supported in part by NASA grants NAGW 2306 and NAG 5-4282.

REFERENCES

Allen, C. W. 1973, Astrophysical Quantities (London: Athlone)
Amado, P. J., & Byrne, P. B. 1996, Irish Astron. J., 23, 177
Appenzeller, I., & Mundt, R. 1989, A&A Rev., 1, 291
Artymowicz, P., & Lubow, S. 1996, ApJ, 467, L77
Basri, G., & Bertout, C. 1989, ApJ, 341, 340
Bell, R. A., & Gustafsson, B. 1989, MNRAS, 236, 653
Bertout, C. 1989, ARA&A, 27, 351
Bertout, C., Basri, G., & Bouvier, J. 1988, ApJ, 330, 350
Bessell, M. S. 1979, PASP, 91, 589
———. 1990, A&AS, 83, 357
———. 1995, in The Bottom of the Main Sequence—and Beyond, ed. C. G. Tinney (Heidelberg: Springer), 129
Bessell, M. S., & Weis, E. W. 1987, PASP, 99, 642
Bouvier, J., Cabrit, S., Fernandez, M., Martin, E. L., & Matthews, J. M. 1993, A&A, 272, 176
Bouvier, J., Covino, E., Kovo, O., Martin, E. L., & Matthews, J. M. 1995, A&A, 299, 89
Camenzind, M. 1990, Rev. in Modern Astronomy 3, ed. G. Klare (Berlin: Springer), 234
D'Antona, F., & Mazzitelli, I. 1994, ApJS, 90, 467
Edwards, S., et al. 1993, AJ, 106, 372
Edwards, S., Hartigan, P., Ghandour, L., & Andralis, C. 1994, AJ, 108, 1056
Ghosh, P., & Lamb, F. K. 1979a, ApJ, 232, 259
———. 1979b, ApJ, 234, 296
Hartigan, P., Edwards, S., & Ghandour, L. 1995, ApJ, 452, 736 (HEG)
Hartigan, P., Hartmann, L., Kenyon, S. J., Hewett, R., & Stauffer, J. 1991, ApJS, 70, 899
Hartigan, P., Hartmann, L., Kenyon, S., Strom, S. E., & Skrutskie, M. F. 1990, ApJ, 354, L25
Hartigan, P., Kenyon, S. J., Hartmann, L., Strom, S. E., Edwards, S., Welty, A. D., & Stauffer, J. 1989, ApJ, 282, 617
Hartmann, L. 1994, in Theory of Accretion Disks 2, ed. W. J. Duschl, J. Frank, F. Meyer, E. Meyer-Hofmeister, & W. M. Tscharnuter (Dordrecht: Kluwer), 19
Hartmann, L., Calvet, N., Gullbring, E., & D'Allessio, P. 1998, ApJ, in press
Hartmann, L., Hewett, R., & Calvet, N. 1994, ApJ, 426, 669
Hatzes, A. P. 1995, ApJ, 451, 784
Herbst, W., Herbst, D. K., & Grossman, E. J. 1994, AJ, 108, 1906
Johnson, H. L. 1966, ARA&A, 3, 193
Joncour, I., Bertout, C., & Bouvier, J. 1994, A&A, 291, L19
Kenyon, S. J., Dobrzycka, D., & Hartmann, L. 1994, AJ, 108, 1872
Kenyon, S. J., & Hartmann, L. 1987, ApJ, 323, 714
———. 1995, ApJS, 101, 117
Königl, A. 1991, ApJ, 370, L39
Legget, S. K., & Hawkins, M. R. S. 1988, MNRAS, 234, 1065
Leinert, C., Zinnecker, H., Weitzel, N., Christou, J., Ridgway, S. T., Jameson, R., & Haas, M. 1993, A&A, 278, 129
Lynden-Bell, D., & Pringle, J. E. 1974, MNRAS, 168, 603
Massey, P., Valdes, F., & Barnes, J. 1992, A User's Guide to Reducing Slit Spectra with IRAF (Tuscon: NOAO)
Mathieu, R. D. 1994, ARA&A, 32, 465
Mathieu, R. D., Stassun, K., Basri, G., Jensen, E. L. N., Johns-Krull, C. M., Valenti, J. A., & Hartmann, L. W. 1997, AJ, 113, 1841
Mathis, J. S. 1990, ARA&A, 28, 37
Muzerolle, J., Calvet, N., & Hartmann, L. 1998, ApJ, in press
Petrov, P. P., Shcherbakov, V. A., Berdyugina, S. V., Shevshenko, V. S., Grankin, K. N., & Melnikov, S. Y. 1994, A&AS, 107, 9
Rice, J. B., & Strassmeier, K. G. 1996, A&A, 316, 164
Shu, F. H., Najita, J., Ruden, S. P., & Lizano, S. 1994, ApJ, 429, 797
Simon, M., Chen, W. P., Howell, R. R., Benson, J. A., & Slowik, D. 1992, ApJ, 384, 212
Strassmeier, K. G., Welty, A. D., & Rice, J. B. 1994, A&A, 285, 17
Thatcher, J. D., & Robinson, R. D. 1993, MNRAS, 262, 1
Thiébaut, E., Balega, Y., Balega, I., Belkine, I., Bouvier, J., Foy, R., Blazit, A., & Bonneau, D. 1995, A&A, 304, L17
Valenti, J. A., Basri, G., & Johns, C. M. 1993, AJ, 106, 2024 (VBJ)
Wang, Y.-M. 1995, ApJ, 449, L153
Weis, E. W. 1993, AJ, 105, 1062